Resolved Single-Molecule Detection of Individual Species within a Mixture of *anti*-Biotin Antibodies Using an Engineered Monomeric Nanopore

Monifa Fahie, Christina Chisholm, and Min Chen*

Molecular and Cellular Biology Program and Department of Chemistry, University of Massachusetts, Amherst, Massachusetts 01003, United States

ABSTRACT Oligomeric protein nanopores with rigid structures have been engineered for the purpose of sensing a wide range of analytes including small molecules and biological species such as proteins and DNA. We chose a monomeric β-barrel porin, OmpG, as the platform from which to derive the nanopore sensor. OmpG is decorated with seven flexible loops that move dynamically to create a distinct gating pattern when ionic current passes through the pore. Biotin was chemically tethered to the most flexible one of these loops. The gating characteristic of the loop's movement in and out of the porin was substantially altered by analyte protein binding. The gating characteristics of the pore with bound targets were remarkably sensitive to molecular identity, even providing the ability to distinguish between homologues within an antibody mixture. A total of five gating parameters were analyzed for each analyte to create a unique fingerprint for each biotin-binding protein. Our exploitation of gating noise as a molecular identifier may allow more sophisticated sensor design, while OmpG's monomeric structure greatly simplifies nanopore production.

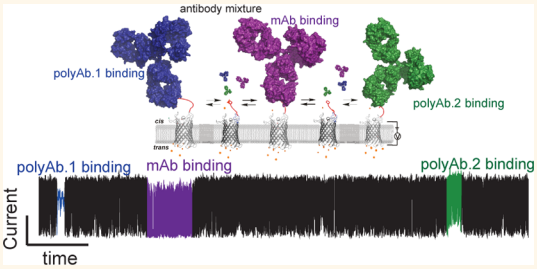

KEYWORDS: nanopore · protein sensor · single-molecule detection · OmpG

Protein nanopores have become powerful single-molecule analytical tools that enable the study of fundamental problems in chemistry and biology,[1,2] including protein folding[3] and unfolding,[4−8] enzymatic activity,[9−11] chemical reactions,[12,13] and stability of complex formation.[14] Beyond basic research, nanopores also hold tremendous promise in biotech applications such as DNA sequencing[11,15−17] and biosensing.[1] Molecular detection using a single nanopore works by observing modulations in ionic current flowing through the pore during an applied potential. Typically, binding (or translocation) of an analyte within (or through) the pore's lumen partially blocks the flow of current and provides information about a molecule's size, concentration, and affinity.[18] Protein nanopores based on protein toxins, especially α-hemolysin (αHL), have been used to detect metal ions,[19,20] organic molecules,[21−23] and oligonucleotides[11,17,24] and to measure the size of polymers.[25,26]

Although αHL works well for small analyte detection, molecules larger than 27 Å in diameter cannot fit in the pore's lumen. Direct protein detection with nanopores is therefore problematic, though some strategies have been developed to transmit the binding signal from solution to the pore's interior.[27−30] For example, binding of a kinase was performed using an αHL pore modified with an inhibitor peptide attached to its stem side.[28] The binding of lethal factor to the PA63 pores of the anthrax toxin orients the N-terminal leader sequence toward the pore's lumen.[31,32] In both cases, analyte docking to the binding site on the sensor pore manifest as a current blockage.[28,32] In addition to direct current blockade, target analytes may also be detected indirectly through current modulation. A common strategy involves a nanopore-permeable molecule, *e.g.*, a small chemical ligand or ligand-modified polymer whose partitioning into or translocation through the nanopore was altered after analyte binding. Following this scheme, the detection of streptavidin or avidin was demonstrated by tethering biotin *via* a PEG

* Address correspondence to mchen1@chem.umass.edu.

Received for review June 18, 2014 and accepted January 9, 2015.

Published online January 09, 2015
10.1021/nn506606e

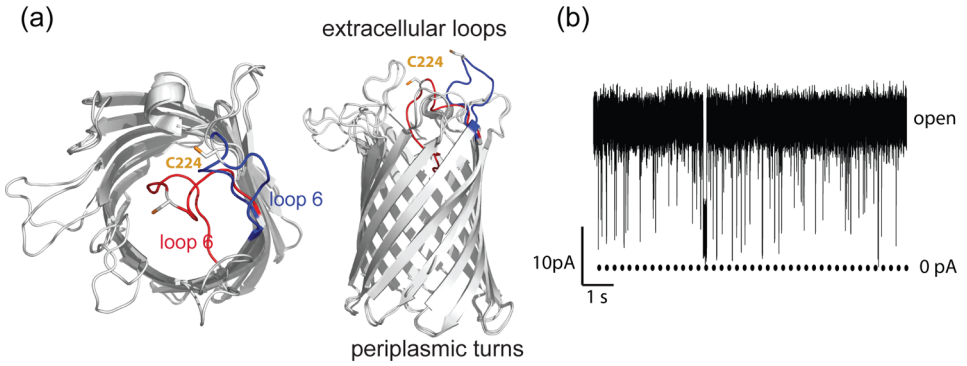

Figure 1. Structures of OmpG and its gating activity. (a) Top view (left) and side view (right) of the structural alignment of the open (2IWV) and closed (2IWW) states. Loop 6 is highlighted in blue in the open state and red in the closed state. The D224C mutation is shown in ball and stick model. (b) Single-channel recording trace of a wild type OmpG pore. The data was obtained in buffer 10 mM Tris·HCl, pH 8.0, 150 mM KCl at +50 mV.

polymer to αHL[30] or monitoring the translocation of biotinylated poly nucleic acids through αHL.[33−35]

Another strategy is to use larger nanopores for analyte detect. For example, the bacterial toxin ClyA, with a 70 Å diameter, was modified at one end with an aptamer specific to thrombin.[36] So far, ClyA represents the largest protein pore for sensing. Although there are many proteins that form larger pores in nature,[37] *e.g.*, perfringolysin O (~15 nm in diameter),[38] their application as sensors has yet to be realized. Synthetic nanopores do not have the size limitation, are more robust,[39−41] and have been applied to identify proteins either during translocation[40−42] or *via* capture by specific receptors immobilized on the wall of the pore.[39,43−45] However, synthetic nanopores lack the well-controlled geometry common to their protein pore counterparts.

Unlike other multimeric proteinaceous nanopores such as αHL and ClyA,[27,36] outer membrane protein G (OmpG) from *Escherichia coli* (*E. coli*) is monomeric.[46] Thus, complex and asymmetric alterations by chemical or genetic modifications are straightforward, making OmpG an attractive nanopore platform for developing nanopore-based sensing technology. OmpG is composed of 14 β-strands connected by seven flexible loops on the extracellular side and seven short turns on the periplasmic side (Figure 1a).[47−49] The extracellular opening is 8 Å in diameter, and the periplasmic side is 14 Å.[50] Wild-type OmpG spontaneously gates during an applied potential as revealed by planar bilayer studies.[46,50] Pore gating is attributed to loop 6 which flops in and out of the pore, intermittently blocking the current (Figure 1a,b).[50,51] To reduce gating, a disulfide bond or lipid anchor was introduced into OmpG's structure, which effectively pinned the flexible loop 6 in place.[50,51] The resulting quiet OmpG was used to sense ADP in the presence of a cyclodextrin adapter.[50]

So far, a rigid and stable structure is usually sought for protein pores for sensing.[2,52] The protein pores with demonstrated sensing applications include αHL,[30] MspA,[53] ClyA,[36] aerolysin,[54] and phi29 DNA packaging motor,[55] all of which are homo-oligomers that possess a rigid structure. Two monomeric outer membrane porins, OmpG[50] and FhuA,[56] with flexible loops have also been used for sensing purposes. However, in both cases the flexible loops were considered as the major obstacle for sensing. These loops were either fixed or removed to stabilize a single open conformation by protein engineering.[50,56] Here, we directly exploit loop dynamics instead of pore blockage to detect protein interactions. Our results demonstrate that the flexibility of Omp*G*'s structure represents a unique feature, which can be used for resolving subtle differences between the surface properties of highly homologous protein analytes. This capability has not been demonstrated with other nanopores.

RESULTS AND DISCUSSION

Detection of Streptavidin by OmpG-PEG$_{11}$-Biotin Pore. To detect proteins, we designed an OmpG nanopore with a ligand tethered to loop 6 to "fish" for target proteins. We hypothesized that target binding would alter the flexibility of loop 6 and, therefore, alter the gating pattern as a recognizable signal to indicate detection. To validate the concept of the OmpG sensor, we first chose biotin and streptavidin as the model ligand and target protein because of its very low dissociation constant of ~10^{-15} M.[57] A single cysteine mutation was introduced to the D224 residue of OmpG by site-directed mutagenesis (Figure 1). The OmpG D224C was expressed in *E. coli* as inclusion bodies and purified by ion-exchange chromatography. Purified OmpG D224C proteins were labeled with maleimide-(PEG)$_{11}$-biotin, and the resulting OmpG-PEG$_{11}$-biotin construct was refolded to its native structure (Figure S1, Supporting Information). The biotin group could extend out from the OmpG pore by approximately 60 Å to facilitate the capture of the analyte proteins (Figure 2a). Single-channel recording of OmpG-D224C and OmpG-PEG$_{11}$-biotin revealed that neither the mutation nor the tethered biotin group induced a measurable

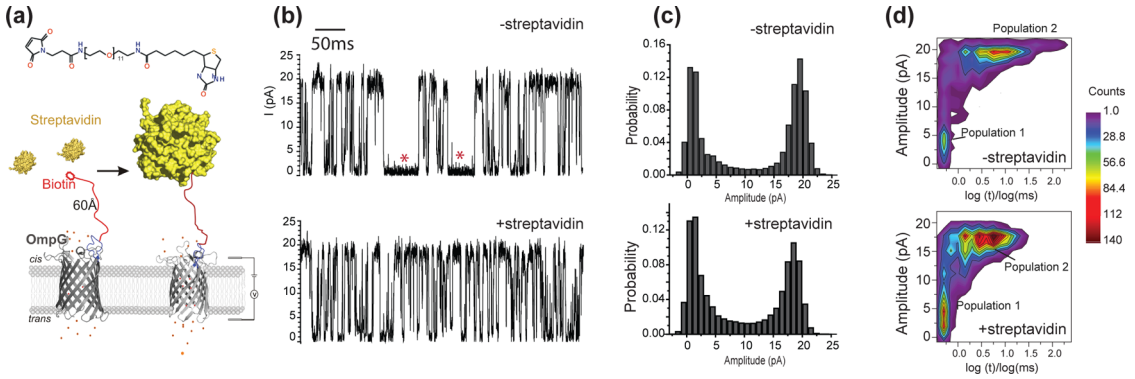

Figure 2. Detection of streptavidin by OmpG-PEG$_{11}$-biotin pore. (a) Schematic model showing the OmpG nanopore chemically modified with maleimide-PEG$_{11}$-biotin. The model was generated in Pymol using PDB files of OmpG (2IWV) and streptavidin (3RY1). The streptavidin was placed approximately 60 Å away from the OmpG pore in the model of the bound state. (b) Representative traces of the OmpG pores before and after the addition of the streptavidin (3 nM). The measurements were performed in buffer 10 mM sodium phosphate, pH5.7, 150 mM KCl at +50 mV. The gating event frequency increases from 75 s^{-1} to 97 s^{-1} after the addition of streptavidin. (c) All current histogram of the corresponding traces in (b). (d) Two-dimensional histogram of the gating events. Gating events collected from a 15s recording trace were distributed based on their intensity *versus* duration. The color scale indicates the number of events.

change in the unitary conductance or gating pattern of OmpG when compared to the wild type protein (Figure S2, Supporting Information). Addition of 3 nM streptavidin to the OmpG-PEG$_{11}$-biotin pore induced an irreversible change in its gating pattern; *i.e.*, a marked increase in gating frequency from 111 ± 30 s^{-1} to 199 ± 27 s^{-1} (n = 3) was observed for OmpG-PEG$_{11}$-biotin pore at pH 5.7 (Figure 2b).

We plot all the gating events according to their gating amplitude and duration in a two-dimensional (2D) event distribution plot (Figure 2d). From the 2D plot analysis, we observe two population of events. Population 1 only partially blocks the pore with amplitudes between 0 to 7.5 pA and dwell time between 0 and 0.4 ms (Figure S3, Supporting Information); population 2 almost fully blocks the pore with amplitudes larger than 10 pA (10−20pA) and dwell time longer than 1 ms (1−50 ms) (Figure S3, Supporting Information). From previous studies and known structures of OmpG,[47,50] we expect that loop 6 cannot fully block the pore on its own as it cannot occupy sufficient space within the lumen. For complete blockage, we expect that as much as one-third of strand 12 must also unfold so that loop 6 is long enough to completely occlude the opening. We give the term "flickering" and "bending" to describe partial *vs* complete blockages, respectively. This distinction is important when considering the behavior observed in the 2D plots. For example, flickering events (population 1) seem relatively constant in the presence or absence of target, while the bending events (population 2) shorten considerably when the target binds (Figure 2d). By contrast, the average dwell time of the bending events decreased from 5.1 ± 0.14 ms to 3.8 ± 0.15 ms (n = 3) (Figure S4, Supporting Information) when streptavidin was bound. In particular, those bending events of especially long duration (>10 ms), indicated with red asterisks, were eliminated during the streptavidin-bound state (Figure 2b,d). We hypothesize that the bending events are shortened by bound streptavidin by destabilizing the closed state. However, due to the increased gating frequency, the open probability of the OmpG pore actually reduced slightly from 0.58 ± 0.09 to 0.51 ± 0.10 (n = 3) upon streptavidin binding as revealed by the decrease of the open state peak (Figure 2c). As controls, streptavidin has also been added to the unmodified OmpG-D224C pores (15 pores tested), we have not observed any change in the gating pattern (Figure S5, Supporting Information). Thus, specific binding of streptavidin to the tethered biotin induces a clear but slight change in the gating properties of OmpG-PEG$_{11}$-biotin pore.

Shortening the Ligand Linker to Strengthen Signal. Since the binding between the OmpG-PEG$_{11}$-biotin and streptavidin produced a relatively small effect on the gating, we hypothesized that the polyethylene linker was too long to effectively restrict the dynamic movement of loop 6. Therefore, we shortened the length of the PEG linker to just two units, creating the OmpG-PEG$_2$-biotin construct where the biotin could extend ∼30 Å into solution (Figure 3a). The shortened linker did not affect the gating pattern when compared to OmpG D224C (Figure S2, Supporting Information). By shortening the linker, the effect of streptavidin binding was much more pronounced, permanently reducing the frequency and amplitude of gating events (Figure 3b,c). Quantitative analysis of three OmpG-PEG$_2$-biotin pores showed that the gating event frequency was reduced by more than 6-fold from 104 ± 6 s^{-1} to 16 ± 2 s^{-1} (n = 3). Comparison of the two-dimensional plots of all events reveals that the occurrence of bending events with long duration time (>0.1 ms) and high intensity (>10 pA) were mostly eliminated due to streptavidin binding (Figure 3d). Gating events of transient duration time (<0.1 μs) and low intensity (<10 pA) still persist albeit with greatly reduced

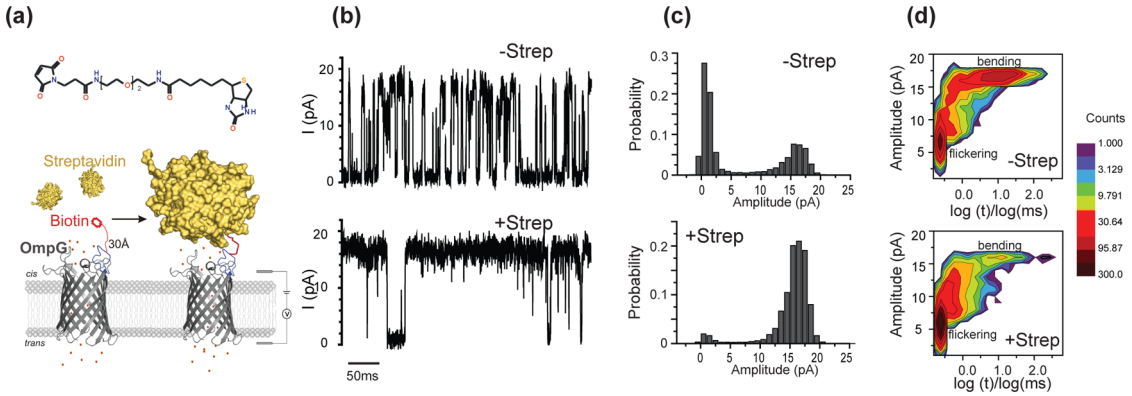

Figure 3. Detection of streptavidin by OmpG-PEG$_2$-biotin pore. (a) Schematic model showing the OmpG nanopore chemically modified with a maleimide-PEG$_2$-biotin. The streptavidin is placed around 30 Å away from the OmpG pore in the model of the bound state. (b) Representative single channel recording traces of the OmpG pores before and after the addition of the streptavidin (3 nM). The measurements were performed in buffer 10 mM sodium phosphate, pH 5.7, 150 mM KCl at +50 mV. (c) All current histogram of the corresponding traces in (b). (d) Two-dimensional histogram of the gating events. Total number of 4000 gating events collected from ~220 and ~40 s recording traces of OmpG pore with and without streptavidin bound were distributed based on their intensity *versus* duration. The color scale indicates the number of the events.

frequency. The data indicate that streptavidin bound to the PEG2 linker can strongly restrict bending but not the flickering of loop 6. As a control, streptavidin was added to OmpG D224C pores and no change was observed (10 pores tested). Adding excess BSA (1 μM) to the OmpG-PEG$_2$-biotin pore also did not show any effect (Figure S6, Supporting Information). These observations confirmed that the alteration of the gating pattern is caused by the specific interaction between the streptavidin and the tethered biotin ligand. In summary, binding of streptavidin to the OmpG-PEG$_2$-biotin nanopore can be detected *via* reduction in gating behavior.

Detection of Reversible Antibody Binding. The biotin–streptavidin interaction is effectively irreversible, thus only one binding event can be detected with the nanopore sensor. Here, we introduce proteins with weaker dissociation constants to look at reversible interactions. Mouse monoclonal antibiotin antibodies (mAb) were added to a recording chamber with a single OmpG-PEG$_2$-biotin (Figure 4a). The electrical trace showed that the presence of biotin-antibody induced a dose-dependent gating pattern that was distinct from the streptavidin bound state (Figure 4b). During antibody binding, the pore shifted to more closed conformation as revealed by the larger closed state peak in the all-current histograms (Figure 4b,c). Indeed, the calculated open probability was reduced from 0.73 ± 0.04 at the no binding state to 0.52 ± 0.04 at the bound state (n = 6). In addition, although the current fluctuates between open and closed states during both the antibody-free and antibody-bound states, the current of the pore in the fully open conformation was slightly reduced by 3.5 ± 0.86 pA (13.6 ± 3.8%, n = 6) during the antibody-bound state compared to the unbound state (Figure 4c). This effect was not observed during the experiments using streptavidin and might suggest that the antibody is in closer proximity to the pore opening when bound. As a control, addition of mAb to OmpGwt and unmodified OmpG D224C pores did not induce any detectable binding signal (Figure S7a, Supporting Information). Neither were mouse antihistag nor *anti*-glyceraldehyde 3-phosphate dehydrogenase (anti-GAPDH) monoclonal antibodies (20 nM) detected by current recording with OmpG-PEG$_2$-biotin pores (Figure S7b, Supporting Information). Thus, these gating events resulted from the specific mAb binding to the tethered biotin.

Next, the dwell time (τ_{off}) and interevent intervals (τ_{on}) of mAb binding was calculated (Figure S8, Supporting Information). The average dissociation rate constant ($k_{off} = 1/\tau_{off}$) of the mAb binding events was 0.25 ± 0.04 s^{-1} (n = 4), which was independent of the antibody concentration (Figure 4d). The observed association constant ($k_{on}' = 1/\tau_{on}$) increased linearly with the increasing concentration of antibody (Figure 4e). The association rate constant k_{on} of antibody binding was 2.30 ± 0.43 × 10^7 $M^{-1}\cdot s^{-1}$ (n = 4). The equilibrium dissociation constant (K_d) of the mouse monoclonal antibody to biotin was 1.12 ± 0.28 × 10^{-8} M^{-1} (n = 4). At the lowest mAb concentration tested (1 nM), the mean interevent interval was 74.5 ± 31 s meaning the OmpG-PEG$_2$-biotin sensor can detect 1 nM antibiotin mAb within tens of min.

Influence of Voltage on the mAb Binding. OmpG exhibits asymmetrical gating pattern at positive and negative voltages. Therefore, we were interested to see if the polarity of the voltage could similarly affect the dynamic motion of loop 6 during the mAb bound state. Figure 5a shows that mAb binds to OmpG-PEG$_2$-biotin at both +50 and −50 mV. The open probability of the mAb bound state at +50 mV and −50 mV is 0.52 ± 0.04 (n = 6) and 0.40 ± 0.09 (n = 6), respectively, in comparison to 0.73 ± 0.04 (n = 6) and 0.71 ± 0.01 (n = 3) of the nonbinding state. Thus, in the mAb-bound state, the pore switched to a slightly more

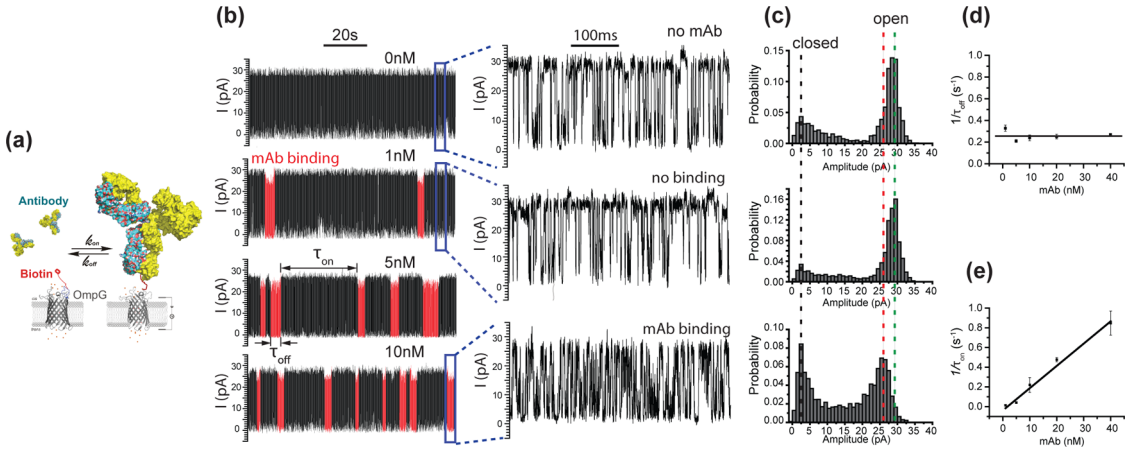

Figure 4. Detection of monoclonal antibiotin antibody by OmpG-PEG$_2$-biotin pore. (a) Schematic model showing the reversible binding of monoclonal antibiotin antibody to OmpG-PEG$_2$-biotin pore. The model is generated in Pymol using pdb files of OmpG (2IWV) and a mouse monoclonal antiphenobarbital antibody (1IGY). The antibody was placed approximately 30 Å away from the OmpG pore in the captured model. (b) Representative single channel recording traces at various mAb concentrations. The mAb binding regions in the recording traces are highlighted in red. Increase of the mAb binding frequency was observed with increasing concentration of mAb. The measurements were performed in buffer 10 mM sodium phosphate, pH 6.0, 300 M KCl at +50 mV. (c) All-current histogram of the corresponding traces in (b). The green and red dashed lines emphasize the shift of the fully open states in current at unoccupied and mAb-bound states, respectively. (d, e) Concentration dependence of the $1/\tau_{off}$ and $1/\tau_{on}$. Error bars represent the standard deviations from the measurements of at least three independent pores.

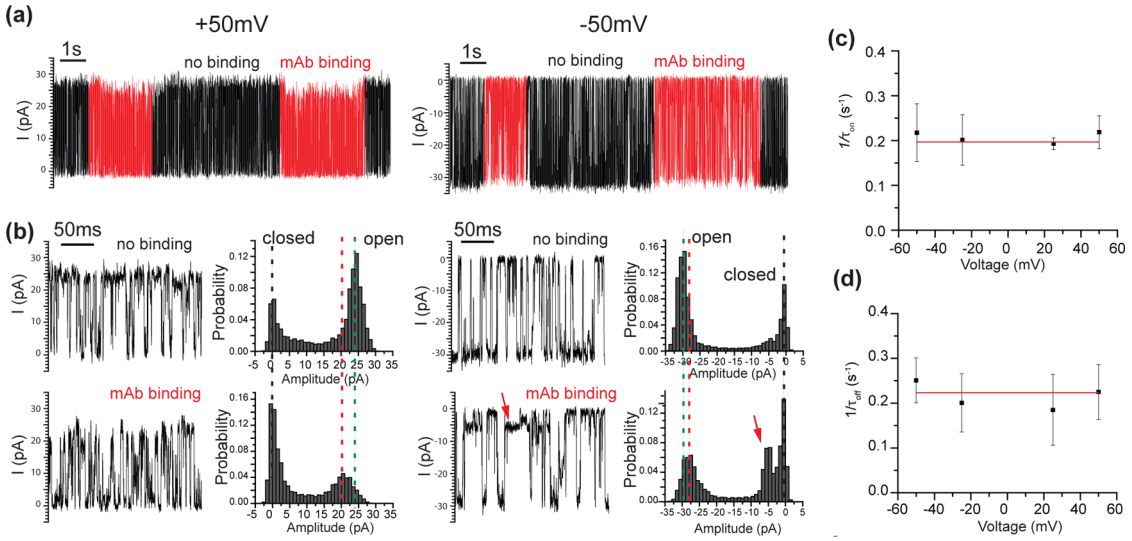

Figure 5. Effect of voltage on the mAb binding. (a) Representative single channel recording trace of OmpG-PEG$_2$-biotin showing reversible binding of the mAb at both +50 mV and −50 mV. We define the positive potential as the potential of the chamber where the loops are located is positive as indicated in (a). The measurement was performed in buffer, 10 mM sodium phosphate buffer, pH 6.0, 300 mM KCl in the presence of 10 nM mAb. (b) Representative single channel recording traces of OmpG-PEG$_2$-biotin at the unoccupied or mAb bound states at +50 and −50 mV. All current histograms of the corresponding current recording traces are also shown. The green and red dashed lines emphasize the shift of the fully open states in current at unoccupied and mAb bound states, respectively. The positive potential caused a larger shift of the open-state current than the negative potential. (c, d) Voltage independence of $1/\tau_{on}$ and $1/\tau_{off}$. The measurements were performed in buffers 10 mM sodium phosphate buffer, pH 6.0, 300 mM KCl in the presence of 10 nM mAb at various applied voltages ranging from −50 to +50 mV.

closed state at the negative potential (Figure 5b). OmpG pore also showed a decreased current by 1.2 ± 0.4 pA (n = 3) at its fully open state at −50 mV. This decrease is ∼5.4% of the current of a no binding state in comparison to the 13.6% decrease at the positive potential. Moreover it had a partial closure state with 6 pA of residual current as indicated by the red arrow in the recording trace and all current histograms (Figure 5b). This result shows that the loop gating during the mAb bound state is still strongly influenced by the polarity of the applied potential. This is a useful feature that can be used for sensing because the asymmetric response of OmpG to target protein binding adds one more parameter for specific analyte protein recognition.

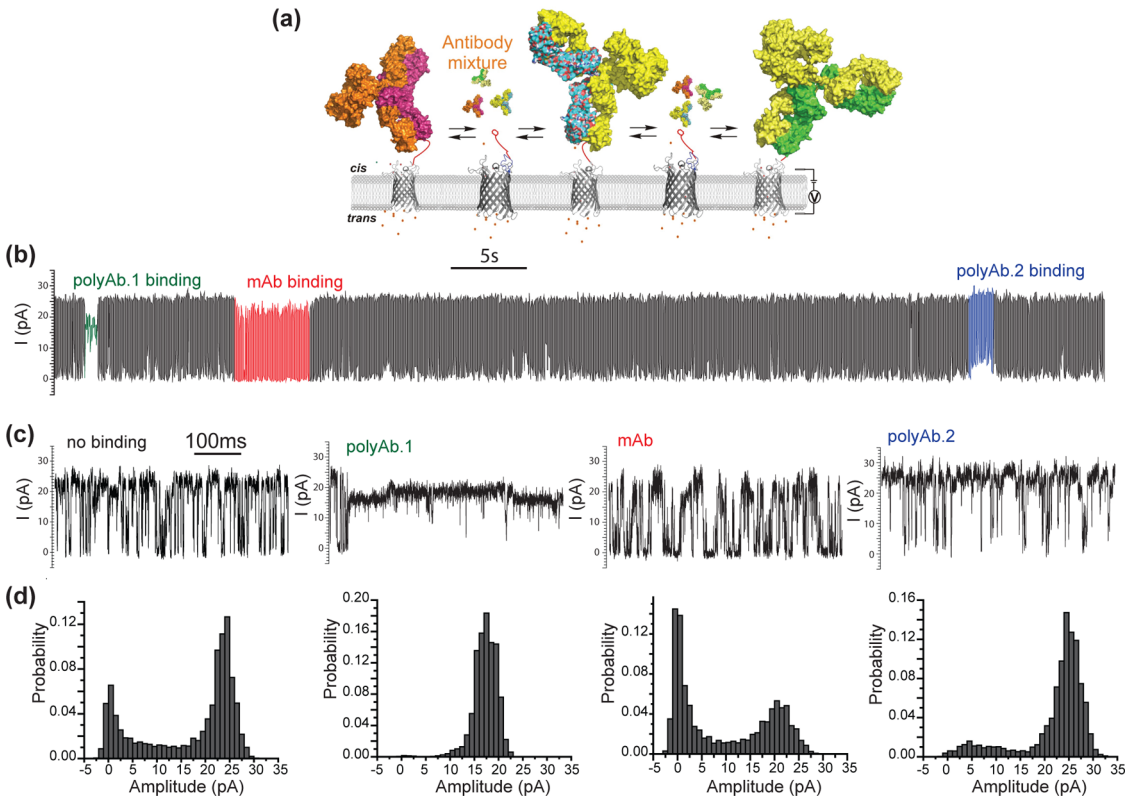

Figure 6. Detection of mouse mAb and polyclonal Ab binding by OmpG-PEG$_2$-biotin pore. (a) Schematic model of simultaneous detection of multiple target proteins by OmpG nanopore. (b) Representative current trace of a single OmpG-biotin. The measurement was performed in the presence of mouse mAb (1 nM) and goat pAb (72 nM) in 10 mM sodium phosphate, pH 6.0, 300 mM KCl at applied potential of +50 mV. The mAb and polyAb binding events are highlighted in colors, *i.e.*, mAb in red, pAb.1 in green, and pAb.2 in blue. (c) Representative current recording trace of OmpG-PEG$_2$-biotin pore at the unoccupied and mAb- and polyAb-bound states. (d) Histograms of the corresponding current recording traces.

Previous studies on nanopore detection have shown that voltage could alter analyte binding kinetics.[28,43,58] Therefore, single-channel recording was performed at applied voltages ranging from −50 to +50 mV in the presence of mouse mAbs. The voltage-dependent gating of OmpG prevented us from testing higher potentials as OmpG tends to close completely at ±75 mV.[46] Neither τ_{on} nor τ_{off} exhibited a strong dependence on voltages (Figure 5c, d) (Figure S9, Supporting Information). Thus, we concluded that the mAb binding to biotin is not affected at applied potentials ranging from −50 to +50 mV. The independence of binding from voltage at this range is advantageous since proteins can be analyzed regardless of the applied potential.

Simultaneous Detection of Mouse mAb and Goat Polyclonal Antibiotin Antibody. Although the antibody and streptavidin both bound the biotinylated OmpG, they produced remarkably unique gating patterns. We wondered how sensitive the OmpG sensor would be to various factors such as a protein's size, shape, surface charge, or rigidity. In an attempt to distinguish between these, we analyzed the binding of a polyclonal antibiotin antibody derived from goat. To our surprise, the polyclonal antibody produced gating patterns distinct from the structurally very similar mAb tested earlier (Figure 6a,b). These specific gating patterns were not observed when polyclonal antibody was added to unmodified OmpG D224C pore (Figure S10, Supporting Information). Furthermore, the polyclonal sample showed clear evidence that at least two readily distinguished populations of antibody were present (Figure 6b,c). We categorized their gating activities into two classes, called types I and II. During type-I binding (pAb.1), the current decreased by 50% and contained few gating events. During type II (pAb.2)-binding events, the open-state conductance was unchanged but the gating frequency was slightly reduced (Figure 6c,d). Mouse mAb was then added to the chamber already containing pAb, and the binding was observed (Figure 6b). All types of antibodies bound with their respective characteristics regardless of the presence of the other antibodies. These gating patterns were not seen when antibodies and streptavidin were added to unmodified OmpG D224C (Figure S11, Supporting Information). This is the first example of a nanopore that can distinguish between three antibodies with virtually identical shape in a complex mixture.

Power Spectrum Analysis and Fingerprint of Analyte Protein Binding Signal. Nanopore sensing often relies on blockade amplitude and/or the mean duration time of

binding to discriminating target molecules. In OmpG nanopore, the binding of analyte not necessarily induced a current blockage. Instead, alteration of the gating/noise of OmpG was indicative of the interaction. Noise spectral density analysis of each biotin-protein bound state revealed that mAb showed a slightly higher noise than the unbound state (Figure 7a and Figure S12, Supporting Information). pAb.1 exhibited the lowest noise while the level of streptavidin, and pAb.2 was between that of pAb.1 and the unbound state. Thus, the noise analysis contributes key information for distinguishing analytes. Noise spectral density analysis of all OmpG pores were also obtained and showed very small changes in noise (Figure S13, Supporting Information)

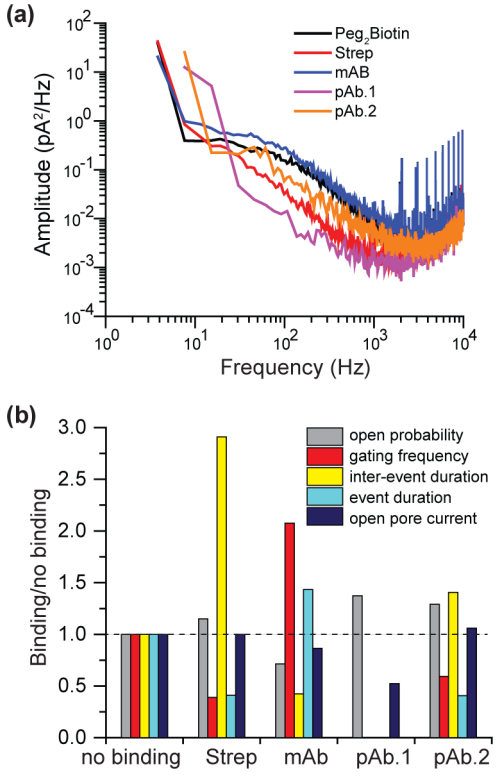

Figure 7. Comparison of the gating patterns of OmpG-PEG_2-biotin at analyte binding states. (a) Power spectra of the protein-binding states for four biotin-binding proteins: streptavidin, mAb, pAb.1, and pAb.2. To compare the streptavidin binding with other biotin-binding proteins under the same conditions, experiments were performed in 10 mM sodium phosphate, pH 6.0, 300 mM KCl (Figure S12, Supporting Information). Electrical traces under this condition were used to derive the power spectra, and the fingerprint characteristics are shown Table 1 and (b). (b) Fingerprints of the biotin binding proteins. The gating events of different analyte protein binding states were characterized by five parameters, *i.e.*, open probability, gating frequency, interevent duration, event duration, and conductance of the open-pore state. Changes of these parameters relative to the no-binding state generate the fingerprint unique for each antibody.

However, noise analysis alone is insufficient for analyte identification. For example, the mAb-bound state was similar to the unbound state, and the open-pore current cannot be seen by noise analysis. To thoroughly analyze the characteristics of the traces at the analyte-binding state, we analyze five parameters: (i) open probability, (ii) gating events frequency, (iii) intergating event duration, (iv) duration of gating events, and (v) the open state conductance to identify the protein (Figure S14, Supporting Information). Table 1 summarizes these parameters, which provide a fingerprint for each analyte (Figure 7b). The OmpG-biotin sensor can unambiguously detect and discriminate between four biotin-binding proteins including three antibody species (two pAb and one mAb) that share highly homologous structures.

DISCUSSION

Since proteins of the same size and shape produce unique signals, we hypothesize that the OmpG sensor recognizes unique targets based on other factors such as charge, hydrophobicity, or perhaps post-translational modification of the surface. The structure of OmpG, along with the data presented here, sheds some light on the possible mechanism of protein detection *via* the nanopore strategy. Although the four biotin-binding proteins trigger a characteristic gating pattern upon binding to the OmpG nanopore, they can be categorized into two groups. In pAb.2 and streptavidin cause a decreased gating frequency, which suggests binding to the PEG_2 tethered biotin hindered the dynamics of the loop 6. According to the crystal structure, the D224 residue traverses approximately 7.5 Å between the open and closed states.[47] However, a recent NMR study of OmpG shows this residue may migrate as far as 30 Å between the fully open and closed conformers.[49,59] Our results suggest that such a large conformational change is strongly hindered by streptavidin binding and moderately by pAb.2 binding. The results also suggest minimal interaction between

TABLE 1. Fingerprint of Each Type of Gating Events

	open probability	event frequency (s^{-1})	interevent duration (ms)	gating duration (ms)	rel conductance of open state (%)
no binding	0.73 ± 0.04[a]	97 ± 3.6	8.68 ± 2.14	2.93 ± 0.52	100
streptavidin	0.95 ± 0.08	45 ± 7	22.75 ± 3.2	0.62 ± 0.19	100 ± 4.2
mAb	0.52 ± 0.04	201 ± 103	3.67 ± 1.57	4.20 ± 1.90	86.4 ± 1.3
pAb.1	0.99 ± 0.01	7 ± 1	n/a	n/a	52.3 ± 4.7
pAb.2	0.94 ± 0.02	57.5 ± 2	12.2 ± 1.3	1.09 ± 0.21	106.5 ± 6.5

[a] Values were calculated from at least three independent experiments. The errors indicate the standard deviation.

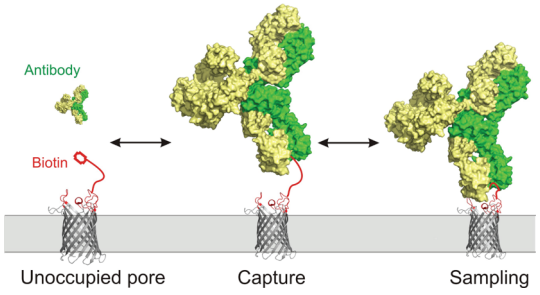

Figure 8. Schematic model illustrating the principle of OmpG nanopore detection.

the streptavidin and pAb.2 with the loops at the opening of OmpG. In another category, mAb and pAb.1 both caused a decrease of current in the fully open state. This observation suggests that the two antibodies obstruct the current flow at the entrance, presumably by partially docking to the extracellular loops of OmpG. Because all seven loops at OmpG's entrance are negatively charged, the two antibodies are likely positively charged or have a positively charged patch near the biotin-binding site that mediate this interaction. This speculation is supported by the observation of mAb's asymmetrical behavior under an applied potential. Namely, a positive potential might push the mAb closer toward the OmpG pore to cause 13.6% partial block of the current (Figure 5) . In contrast, at negative potential, the electric field would repel mAb away from the pore entrance. Indeed, we observed that the open pore conductance was less affected, only ~5.4% blockage seen. These results suggest that not only the ligand-tethered loop, but all the loops on the extracellular entrance may be involved in interacting and sampling the target proteins, which explains its ability to discriminate between highly structurally homologous proteins. We expect the interaction between the loops and the two antibodies is weak because mAb and pAb.1 did not induce noticeable changes to the gating of unlabeled OmpG D224C. However, these interactions may be enhanced after the antibodies bind the tethered biotin ligand. In summary, our data suggests a novel mechanism underlying OmpG nanopore sensing that contains two steps (Figure 8). First, OmpG captures the target protein *via* its tethered high-affinity ligand. Consequently, the bound protein interferes with the movement of loop 6 generating its characteristic gating pattern. Second, the extracellular loops of OmpG may sample the target protein *via* unspecific interactions which further alters the ionic current providing additional readout. While further study is required to delve deeper into the precise mechanism of protein detection, our sensor's ability to discriminate between structurally homologous antibodies within a multicomponent mixture represents a powerful advance over previous approaches.

Previously, the detection of streptavidin and antibiotin antibody was demonstrated using αHL that contained a PEG biotin group tethered to its vestibule.[30] In the absence of the target, the PEG polymer traversed through the constriction site from the *cis* and *trans* chamber and back through the pore. This movement was manifest as rapid gating. Analyte protein binding of the biotin group eliminated the gating and provided the readout signal for protein sensing. In contrast to our OmpG nanopore, αHL-biotin sensor did not differentiate binding events derived from streptavidin and mAb which differ greatly in size, shape and surface properties. Two features of OmpG may contribute to its higher resolution compared to αHL (Figure S15, Supporting Information). The first is the location of the constriction site which is the narrowest part of the pore that determines the conductance. The constriction site of OmpG-PEG_2-biotin is located at the entrance to the pore next to the ligand interaction site while the location of the constriction site of αHL is in the middle making it inaccessible for large folded analyte protein. Because of this, analyte protein binding at the pore entrance directly affected the conductance of OmpG but not αHL. Second OmpG has flexible loops at the binding site which allows conformational changes to occur in response to analyte protein binding. Instead, αHL possesses a rather stable and rigid structure at the two ends.[60] Although the biotin-binding proteins might also interact with the two entrances of αHL nanopore, the rigidity of the αHL structure does not allow large conformational changes to occur, so the interaction of different target proteins with the entrance did not induce noticeable changes in the current flow that passed through the constriction site.

Our study points out an alternative design in the architecture of nanopore sensors. By creating a nanopore with a dynamic structure that changes upon analyte binding, new regions of data may be interpreted that give a greater sensitivity and selectivity for detecting protein analytes. We have shown that even protein isoforms in a mixture can be clearly distinguished using this new sensing scheme. These features are not available in other nanopore sensing strategies, making the OmpG sensor particularly useful. Further, monomeric proteins such as OmpG are ready to use after refolding and require no further assembly and purification steps compared to other oligomeric nanopores.

CONCLUSION

We have shown that binding of target protein to an OmpG-biotin nanopore can be deduced from changes in the gating activity of OmpG. The principle of the OmpG nanopore relies on detecting the modulation of loop dynamics upon target protein binding rather than the occupation in the pore lumen. More importantly,

the OmpG nanopore exhibited the ability to resolve protein homologues that share the same high-affinity ligand, making this sensing approach well suitable for screening for homologous disease markers in complex mixtures. In the future, this principle may be extended to a broader spectrum of analytes, such as proteins, viruses, or bacteria, without the need to use a far larger nanopore.

METHODS

Single-Channel Recording of OmpG Proteins. Single-channel recording of OmpG was similar to the previous study.[50] Briefly, experiments were performed in an apparatus containing two chambers separated by a 25 μm thick Teflon film. An aperture of approximately 100 μm diameter had been made near the center of the film with an electric spark. The aperture was pretreated with a hexadecane/pentane (10% v/v) solution before each chamber was filled with buffers as indicated specifically. An Ag/AgCl electrode was immersed in each chamber with the *cis* chamber grounded. 1,2-Diphytanoyl-*sn*-glycerol-3-phosphocholine (Avanti Polar Lipids, USA) dissolved in pentane (10 mg/mL) was deposited on the surface of the buffer in both chambers and monolayers formed after the pentane evaporated. The lipid bilayer was formed by raising the liquid level up and down across the aperture. OmpG proteins ($\sim$1 nM, final concentration) were added to the *cis* chamber, and +200 mV was applied to facilitate OmpG insertion. After a single OmpG pore inserted, the applied voltage was lowered to 50 mV for recording. OmpG proteins inserted in the planar lipid bilayer bidirectionally with its extracellular loops located at either *cis* or *trans* side. After 10 min recording, the orientation of the OmpG pore in the lipid bilayer was determined by analyzing the asymmetrical gating pattern at positive and negative potentials.[61] Streptavidin or antibodies were added to the *cis* or *trans* chamber depending on the pore orientation and the solution was stirred for 10 s. We define a positive potential as the potential of the chamber where the extracellular loops were exposed to is positive. Current was amplified with an Axopatch 200B integrating patch clamp amplifier (Axon Instruments, Foster City, CA). Signals were filtered with a Bessel filter at 2 kHz (unless otherwise stated) and then acquired by a computer (sampling at 50 μs) after digitization with a Digidata 1320A/D board (Axon Instruments).

Single-Channel Current Analysis. For power spectra analysis, data were recorded with a Bessel filter at 50 kHz and acquired at 250 kHz. Power spectra were calculated from a 20 s recording trace in Clampfit using segment lengths of 32768 samples (spectra resolution 7.62 Hz) by applying the Hamming window. Data shown were derived from averaged spectra segments with 50% window overlap. To analyze the mAb and polyclonal antibody binding, power spectra of multiple binding events from a total of 20 s recording time were calculated and averaged. The power spectra densities for all traces were plotted in OriginPro 9.1.

Conflict of Interest: The authors declare no competing financial interest.

Supporting Information Available: Full documentation of materials; mutagenesis of OmpG; preparation of biotin-labeled OmpG pore; analysis of the duration of bending events before and after streptavidin binding; details of fingerprint analysis of antibody binding; comparison of αHL and OmpG. This material is available free of charge *via* the Internet at http://pubs.acs.org

Acknowledgment. M.F. was supported in part by a Fellowship from the University of Massachusetts as part of the Chemistry−Biology Interface training grant (T32 GM08515).

REFERENCES AND NOTES

1. Howorka, S.; Siwy, Z. Nanopore Analytics: Sensing of Single Molecules. *Chem. Soc. Rev.* **2009**, *38*, 2360–2384.
2. Majd, S.; Yusko, E. C.; Billeh, Y. N.; Macrae, M. X.; Yang, J.; Mayer, M. Applications of Biological Pores in Nanomedicine, Sensing, and Nanoelectronics. *Curr. Opin Biotechnol* **2010**, *21*, 439–476.
3. Stefureac, R. I.; Lee, J. S. Nanopore Analysis of the Folding of Zinc Fingers. *Small* **2008**, *4*, 1646–1650.
4. Merstorf, C.; Cressiot, B.; Pastoriza-Gallego, M.; Oukhaled, A.; Betton, J. M.; Auvray, L.; Pelta, J. Wild Type, Mutant Protein Unfolding and Phase Transition Detected by Single-Nanopore Recording. *ACS Chem. Biol.* **2012**, *7*, 652–658.
5. Nivala, J.; Marks, D. B.; Akeson, M. Unfoldase-Mediated Protein Translocation through an Alpha-Hemolysin Nanopore. *Nat. Biotechnol.* **2013**, *31*, 247–250.
6. Oukhaled, G.; Mathe, J.; Biance, A. L.; Bacri, L.; Betton, J. M.; Lairez, D.; Pelta, J.; Auvray, L. Unfolding of Proteins and Long Transient Conformations Detected by Single Nanopore Recording. *Phys. Rev. Lett.* **2007**, *98*, 158101.
7. Payet, L.; Martinho, M.; Pastoriza-Gallego, M.; Betton, J. M.; Auvray, L.; Pelta, J.; Mathe, J. Thermal Unfolding of Proteins Probed at the Single Molecule Level Using Nanopores. *Anal. Chem.* **2012**, *84*, 4071–4076.
8. Rodriguez-Larrea, D.; Bayley, H. Multistep Protein Unfolding During Nanopore Translocation. *Nat. Nanotechnol.* **2013**, *8*, 288–295.
9. Majd, S.; Yusko, E. C.; MacBriar, A. D.; Yang, J.; Mayer, M. Gramicidin Pores Report the Activity of Membrane-Active Enzymes. *J. Am. Chem. Soc.* **2009**, *131*, 16119–16126.
10. Zhao, Q.; de Zoysa, R. S.; Wang, D.; Jayawardhana, D. A.; Guan, X. Real-Time Monitoring of Peptide Cleavage Using a Nanopore Probe. *J. Am. Chem. Soc.* **2009**, *131*, 6324–6325.
11. Kasianowicz, J. J.; Brandin, E.; Branton, D.; Deamer, D. W. Characterization of Individual Polynucleotide Molecules Using a Membrane Channel. *Proc. Natl. Acad. Sci. U.S.A.* **1996**, *93*, 13770–13773.
12. Luchian, T.; Shin, S. H.; Bayley, H. Single-Molecule Covalent Chemistry with Spatially Separated Reactants. *Angew. Chem., Int. Ed.* **2003**, *42*, 3766–3771.
13. Shin, S. H.; Luchian, T.; Cheley, S.; Braha, O.; Bayley, H. Kinetics of a Reversible Covalent-Bond-Forming Reaction Observed at the Single-Molecule Level. *Angew. Chem., Int. Ed.* **2002**, *41*, 3707–37093523.
14. Arnaut, V.; Langecker, M.; Simmel, F. C. Nanopore Force Spectroscopy of Aptamer-Ligand Complexes. *Biophys. J.* **2013**, *105*, 1199–1207.
15. Branton, D.; Deamer, D. W.; Marziali, A.; Bayley, H.; Benner, S. A.; Butler, T.; Di Ventra, M.; Garaj, S.; Hibbs, A.; Huang, X.; et al. The Potential and Challenges of Nanopore Sequencing. *Nat. Biotechnol.* **2008**, *26*, 1146–1153.
16. Wanunu, M. Nanopores: A Journey Towards DNA Sequencing. *Phys. Life Rev.* **2012**, *9*, 125–158.
17. Meller, A.; Nivon, L.; Brandin, E.; Golovchenko, J.; Branton, D. Rapid Nanopore Discrimination between Single Polynucleotide Molecules. *Proc. Natl. Acad. Sci. U.S.A.* **2000**, *97*, 1079–1084.
18. Bayley, H.; Cremer, P. S. Stochastic Sensors Inspired by Biology. *Nature* **2001**, *413*, 226–230.
19. Braha, O.; Gu, L. Q.; Zhou, L.; Lu, X.; Cheley, S.; Bayley, H. Simultaneous Stochastic Sensing of Divalent Metal Ions. *Nat. Biotechnol.* **2000**, *18*, 1005–1007.
20. Braha, O.; Walker, B.; Cheley, S.; Kasianowicz, J. J.; Song, L.; Gouaux, J. E.; Bayley, H. Designed Protein Pores as Components for Biosensors. *Chem. Biol.* **1997**, *4*, 497–505.
21. Cheley, S.; Gu, L. Q.; Bayley, H. Stochastic Sensing of Nanomolar Inositol 1,4,5-Trisphosphate with an Engineered Pore. *Chem. Biol.* **2002**, *9*, 829–838.
22. Wu, H. C.; Bayley, H. Single-Molecule Detection of Nitrogen Mustards by Covalent Reaction within a Protein Nanopore. *J. Am. Chem. Soc.* **2008**, *130*, 6813–6819.

23. Gu, L. Q.; Braha, O.; Conlan, S.; Cheley, S.; Bayley, H. Stochastic Sensing of Organic Analytes by a Pore-Forming Protein Containing a Molecular Adapter. *Nature* **1999**, *398*, 686–690.
24. Howorka, S.; Cheley, S.; Bayley, H. Sequence-Specific Detection of Individual DNA Strands Using Engineered Nanopores. *Nat. Biotechnol.* **2001**, *19*, 636–639.
25. Reiner, J. E.; Kasianowicz, J. J.; Nablo, B. J.; Robertson, J. W. Theory for Polymer Analysis Using Nanopore-Based Single-Molecule Mass Spectrometry. *Proc. Natl. Acad. Sci. U.S.A.* **2010**, *107*, 12080–12085.
26. Robertson, J. W.; Rodrigues, C. G.; Stanford, V. M.; Rubinson, K. A.; Krasilnikov, O. V.; Kasianowicz, J. J. Single-Molecule Mass Spectrometry in Solution Using a Solitary Nanopore. *Proc. Natl. Acad. Sci. U.S.A.* **2007**, *104*, 8207–8211.
27. Rotem, D.; Jayasinghe, L.; Salichou, M.; Bayley, H. Protein Detection by Nanopores Equipped with Aptamers. *J. Am. Chem. Soc.* **2012**, *134*, 2781–2787.
28. Xie, H.; Braha, O.; Gu, L. Q.; Cheley, S.; Bayley, H. Single-Molecule Observation of the Catalytic Subunit of Camp-Dependent Protein Kinase Binding to an Inhibitor Peptide. *Chem. Biol.* **2005**, *12*, 109–120.
29. Howorka, S.; Nam, J.; Bayley, H.; Kahne, D. Stochastic Detection of Monovalent and Bivalent Protein-Ligand Interactions. *Angew. Chem., Int. Ed.* **2004**, *43*, 842–846.
30. Movileanu, L.; Howorka, S.; Braha, O.; Bayley, H. Detecting Protein Analytes That Modulate Transmembrane Movement of a Polymer Chain within a Single Protein Pore. *Nat. Biotechnol.* **2000**, *18*, 1091–1095.
31. Zhang, S.; Udho, E.; Wu, Z.; Collier, R. J.; Finkelstein, A. Protein Translocation through Anthrax Toxin Channels Formed in Planar Lipid Bilayers. *Biophys. J.* **2004**, *87*, 3842–3849.
32. Halverson, K. M.; Panchal, R. G.; Nguyen, T. L.; Gussio, R.; Little, S. F.; Misakian, M.; Bavari, S.; Kasianowicz, J. J. Anthrax Biosensor, Protective Antigen Ion Channel Asymmetric Blockade. *J. Biol. Chem.* **2005**, *280*, 34056–34062.
33. Henrickson, S. E.; DiMarzio, E. A.; Wang, Q.; Stanford, V. M.; Kasianowicz, J. J. Probing Single Nanometer-Scale Pores with Polymeric Molecular Rulers. *J. Chem. Phys.* **2010**, *132*, 135101.
34. Henrickson, S. E.; Misakian, M.; Robertson, B.; Kasianowicz, J. J. Driven DNA Transport into an Asymmetric Nanometer-Scale Pore. *Phys. Rev. Lett.* **2000**, *85*, 3057–3060.
35. Kasianowicz, J. J.; Henrickson, S. E.; Weetall, H. H.; Robertson, B. Simultaneous Multianalyte Detection with a Nanometer-Scale Pore. *Anal. Chem.* **2001**, *73*, 2268–2272.
36. Soskine, M.; Biesemans, A.; Moeyaert, B.; Cheley, S.; Bayley, H.; Maglia, G. An Engineered Clya Nanopore Detects Folded Target Proteins by Selective External Association and Pore Entry. *Nano Lett.* **2012**, *12*, 4895–4900.
37. Rosado, C. J.; Kondos, S.; Bull, T. E.; Kuiper, M. J.; Law, R. H.; Buckle, A. M.; Voskoboinik, I.; Bird, P. I.; Trapani, J. A.; Whisstock, J. C.; et al. The Macpf/Cdc Family of Pore-Forming Toxins. *Cell Microbiol.* **2008**, *10*, 1765–1774.
38. Olofsson, A.; Hebert, H.; Thelestam, M. The Projection Structure of Perfringolysin O (Clostridium Perfringens Theta-Toxin). *FEBS Lett.* **1993**, *319*, 125–127.
39. Siwy, Z.; Trofin, L.; Kohli, P.; Baker, L. A.; Trautmann, C.; Martin, C. R. Protein Biosensors Based on Biofunctionalized Conical Gold Nanotubes. *J. Am. Chem. Soc.* **2005**, *127*, 5000–5001.
40. Han, A.; Schürmann, G.; Mondin, G.; Bitterli, R. A.; Hegelbach, N. G.; de Rooij, N. F.; Staufer, U. Sensing Protein Molecules Using Nanofabricated Pores. *Appl. Phys. Lett.* **2006**, *88*, 093901.
41. Li, W.; Bell, N. A.; Hernandez-Ainsa, S.; Thacker, V. V.; Thackray, A. M.; Bujdoso, R.; Keyser, U. F. Single Protein Molecule Detection by Glass Nanopores. *ACS Nano* **2013**, *7*, 4129–4134.
42. Fologea, D.; Ledden, B.; McNabb, D. S.; Li, J. Electrical Characterization of Protein Molecules by a Solid-State Nanopore. *Appl. Phys. Lett.* **2007**, *91*, 539011–539013.
43. Wei, R.; Gatterdam, V.; Wieneke, R.; Tampe, R.; Rant, U. Stochastic Sensing of Proteins with Receptor-Modified Solid-State Nanopores. *Nat. Nanotechnol* **2012**, *7*, 257–263.
44. Ding, S.; Gao, C.; Gu, L. Q. Capturing Single Molecules of Immunoglobulin and Ricin with an Aptamer-Encoded Glass Nanopore. *Anal. Chem.* **2009**, *81*, 6649–6655.
45. Yusko, E. C.; Johnson, J. M.; Majd, S.; Prangkio, P.; Rollings, R. C.; Li, J.; Yang, J.; Mayer, M. Controlling Protein Translocation through Nanopores with Bio-Inspired Fluid Walls. *Nat. Nanotechnol.* **2011**, *6*, 253–260.
46. Conlan, S.; Zhang, Y.; Cheley, S.; Bayley, H. Biochemical and Biophysical Characterization of Ompg: A Monomeric Porin. *Biochemistry* **2000**, *39*, 11845–11854.
47. Yildiz, O.; Vinothkumar, K. R.; Goswami, P.; Kuhlbrandt, W. Structure of the Monomeric Outer-Membrane Porin Ompg in the Open and Closed Conformation. *EMBO J.* **2006**, *25*, 3702–3713.
48. Subbarao, G. V.; van den Berg, B. Crystal Structure of the Monomeric Porin Ompg. *J. Mol. Biol.* **2006**, *360*, 750–759.
49. Liang, B.; Tamm, L. K. Structure of Outer Membrane Protein G by Solution Nmr Spectroscopy. *Proc. Natl. Acad. Sci. U.S. A.* **2007**, *104*, 16140–16145.
50. Chen, M.; Khalid, S.; Sansom, M. S.; Bayley, H. Outer Membrane Protein G: Engineering a Quiet Pore for Biosensing. *Proc. Natl. Acad. Sci. U.S.A.* **2008**, *105*, 6272–6277.
51. Zhuang, T.; Tamm, L. K. Control of the Conductance of Engineered Protein Nanopores through Concerted Loop Motions. *Angew. Chem., Int. Ed.* **2014**, *53*, 5897–5902.
52. Movileanu, L. Interrogating Single Proteins through Nanopores: Challenges and Opportunities. *Trends Biotechnol.* **2009**, *27*, 333–341.
53. Butler, T. Z.; Pavlenok, M.; Derrington, I. M.; Niederweis, M.; Gundlach, J. H. Single-Molecule DNA Detection with an Engineered Mspa Protein Nanopore. *Proc. Natl. Acad. Sci. U.S.A.* **2008**, *105*, 20647–20652.
54. Pastoriza-Gallego, M.; Rabah, L.; Gibrat, G.; Thiebot, B.; van der Goot, F. G.; Auvray, L.; Betton, J.-M.; Pelta, J. Dynamics of Unfolded Protein Transport through an Aerolysin Pore. *J. Am. Chem. Soc.* **2011**, *133*, 2923–2931.
55. Wendell, D.; Jing, P.; Geng, J.; Subramaniam, V.; Lee, T. J.; Montemagno, C.; Guo, P. Translocation of Double-Stranded DNA through Membrane-Adapted Phi29 Motor Protein Nanopores. *Nat. Nanotechnol* **2009**, *4*, 765–772.
56. Mohammad, M. M.; Iyer, R.; Howard, K. R.; McPike, M. P.; Borer, P. N.; Movileanu, L. Engineering a Rigid Protein Tunnel for Biomolecular Detection. *J. Am. Chem. Soc.* **2012**, *134*, 9521–9531.
57. Green, N. M. Avidin and Streptavidin. *Methods Enzymol.* **1990**, *184*, 51–67.
58. Gu, L. Q.; Bayley, H. Interaction of the Noncovalent Molecular Adapter, Beta-Cyclodextrin, with the Staphylococcal Alpha-Hemolysin Pore. *Biophys. J.* **2000**, *79*, 1967–1975.
59. Zhuang, T.; Chisholm, C.; Chen, M.; Tamm, L. K. Nmr-Based Conformational Ensembles Explain Ph-Gated Opening and Closing of Ompg Channel. *J. Am. Chem. Soc.* **2013**, *135*, 15101–15113.
60. Song, L.; Hobaugh, M. R.; Shustak, C.; Cheley, S.; Bayley, H.; Gouaux, J. E. Structure of Staphylococcal Alpha-Hemolysin, a Heptameric Transmembrane Pore. *Science* **1996**, *274*, 1859–1866.
61. Chen, M.; Li, Q. H.; Bayley, H. Orientation of the Monomeric Porin Ompg in Planar Lipid Bilayers. *ChemBioChem* **2008**, *9*, 3029–3036.